JOURNAL OF GEOPHYSICAL RESEARCH, SPACE PHYSICS VOL. 75, NO. 1, JANUARY 1, 1970

Satellite Observations of Equatorial Phenomena and Defocusing of VLF Electromagnetic Waves

R. R. SCARABUCCI

Radioscience Laboratory
Stanford University, Stanford, California 94305

Amplitude measurements of whistlers and signals from VLF transmitters have been made with the low altitude, polar-orbiting OGO 4 satellite. Two aspects of these measurements related to the behavior of the waves near the magnetic equator are described and interpreted: (1) Daytime spectrograms taken near the magnetic equator show a remarkable high-frequency cutoff in the amplitude of the VLF whistler waves. The cutoff frequency decreases as the satellite approaches the magnetic equator, and sometimes all signals drop below the equipment threshold. This feature is also present when the signals from different VLF transmitters are simultaneously observed. It is shown that the above phenomenon is explained primarily by absorption in the D and E regions of the ionosphere and by the daytime ray trajectories near the equator. (2) During the night, absorption becomes relatively small, but nevertheless an abrupt amplitude cutoff of signals from VLF transmitters may still occur. This nighttime cutoff is explained primarily by defocusing near the equator, which is enhanced for nighttime ionization profiles. The defocusing of the VLF waves depends strongly upon the rapid change of ionization-gradient occurring between 500 and 1000 km of height and also upon the curvature of the earth's magnetic field around the magnetic equator.

INTRODUCTION

The purpose of this paper is to present and discuss two new ionospheric phenomena involving the propagation and absorption of VLF waves near the magnetic equator. Both phenomena are related to attenuation of VLF signals received aboard a polar orbiting satellite when the spacecraft travels at low latitudes. One effect, called 'equatorial erosion,' occurs on the dayside and involves frequency-dependent attenuation, with all VLF signals from ground sources eventually disappearing below the level of detectability as the satellite approaches the equator. An example of equatorial erosion observed from OGO 4 is shown in Figure 1 (see page 81), which displays frequency from 0 to 10 kHz versus magnetic latitude and time on a northbound pass. As the satellite moves toward the equator between 2049 and 2050 UT, broadband VLF whistler signals are 'eroded,' cutting off at successively lower frequencies with decreasing latitude. The activity recovers north of the equator, but in somewhat irregular fashion.

The other new phenomenon, interpreted here as 'equatorial defocusing,' is observed in the nighttime ionosphere and involves abrupt decreases in the intensity of manmade VLF signals, typically more than 15 db in less than 50 km. Two examples of equatorial defocusing are shown by the OGO 4 records of Figure 2 (see page 82). The two panels show for two consecutive nighttime equatorial passes the amplitude of the magnetic field of signals transmitted by NAA (17.8 kHz) and received aboard the satellite by a phase tracking receiver. The records show NAA signal levels of about -80 to -90 dbγ (i.e., db relative to 1 gamma; 1 $\gamma = 7.96 \times 10^{-4}$ amp/m) when the satellite is at geographic latitudes of about $-25°$, and as the satellite moves northward a pronounced drop in signal intensity occurs at the vicinity of $-20°$ with the field strength dropping below the noise level of about -100 dbγ. The signal remains below the noise level in the succeeding 15° of northward satellite flight and emerges from the noise at a geographic latitude of about $-5°$.

Very-low-frequency waves were first observed in the magnetosphere in 1961 by the Lofti 1 satellite [*Leiphart et al.*, 1962]. In this experiment VLF signals were received from Navy stations NBA in the Canal Zone and NPG in Jim Creek, Washington. Interpreting these measurements, *Rorden et al.* [1964] reported a

higher attenuation in the signals from NBA, and suggested that the difference could be attributed to a greater absorption at low latitudes. A more systematic observation of this kind was reported by *Heyborne* [1966], who studied the continuous reception aboard the OGO 2 satellite of VLF signals from NPG and NAA. The records showed a consistent drop of the VLF wavefields at each satellite pass over the equator. It was shown that this effect could be attributed to higher ionospheric absorption around the equator.

Better observations of equatorial phenomena have been obtained from the stabilized satellite OGO 4, which provides repeatability of measurements and more confidence in data analysis. Data interpretation has been aided by a new approach involving a full-wave study of the transmission coefficient in the lower ionosphere and a ray-tracing technique to determine effects such as defocusing of the power flow. This approach has led to a satisfactory interpretation of the data, in which the roles of absorption and defocusing in the day and night regimes have been separately identified.

The present paper will show that the equatorial erosion is caused by the combined effect of high absorption in the D region at low latitudes plus the ray trajectories followed by the signals above the F region. At night the absorption effect is less important, with low-altitude equatorial propagation being dominated by a pronounced ionospheric defocusing caused by a rapid increase of the electron-concentration scale-height above about 500 km. It will be shown that the defocusing phenomenon represents a method of detecting large variations in the vertical gradient of electron concentration. Therefore, this effect may be used for measuring the nighttime $[O^+ - H^+]$ transition height at the equator.

Brief description of the experiment. OGO 4 is a polar orbiting satellite whose period is of the order of 100 minutes. Height varies from approximately 400 to 900 km, and the orbit inclination is 86°. The Stanford University/Stanford Research Institute experiment aboard OGO 4 consists of a loop antenna, preamplifier, 3 narrowband receivers, 2 broadband receivers, and one phase tracking receiver. The preamplifier drives the receivers with a spectrum ranging from 30 Hz to 100 kHz. The three amplitude-calibrated narrowband receivers may be tuned to prescribed frequencies, or they may synchronously sweep in frequency from the bottom to the top of the 3 bands, 0.13 to 1.56 kHz, 1.05 to 12.5 kHz, and 8.4 to 100 kHz. The broadband receivers provide spectral information in the range 30 to 300 Hz (ELF channel) and 0.3 to 12.5 kHz (VLF channel). The phase tracking receiver measures amplitude and phase of waves in a sharp-edged passband of 50 Hz width for frequencies between 14 and 27 kHz

The Equatorial Erosion

The equatorial erosion effect is manifested in every one of about 200 OGO 4 records of equatorial crossings obtained in daytime during 1967 and 1968. Frequency-time records such as those of Figure 1 typically show that as the satellite approaches the equator the highest frequencies disappear first. Although Figure 1 is typical with respect to the sharpness of the cutoff south of the equator, it shows an unusually smooth variation as compared with most records. Sometimes the erosion is not complete, and the lowest whistler frequencies are observed throughout the equatorial crossing. The erosion effect is also consistently observed at the output of the narrowband receivers when these receivers are working in the 'sweeping mode.' It is then usually observed as a disappearance of all ground-source VLF signals from 0.13 to 100 kHz.

Qualitative explanation of the observations. The equatorial erosion may be understood in terms of an increase in the transmission loss through the ionosphere with decreasing magnetic latitude. In daytime all VLF waves propagate upward with nearly vertical wave normals, a consequence of applying Snell's law to the lower stratified layers of the ionosphere. Hence, in the region of high VLF absorption (70–80 km), the angle between the wave normals and the earth's magnetic field increases as the satellite approaches the equator. The medium becomes optically thicker, which means that the electrical length of the wave train inside the medium increases, and therefore the wave experiences greater collisional absorption. Thus for a collision-frequency constant in latitude, the absorption should become greater at lower latitudes.

Above 100 km the ionosphere is a slowly

varying medium for all VLF waves, and geometrical optics may be applied in order to determine the path followed by a wave packet. The ray trajectories are not symmetrical around the equator which, as will be seen, accounts partially for the nonsymmetrical properties of the erosion effects displayed in Figure 1. In fact, daytime propagation around the magnetic equator is influenced primarily by the high vertical gradient of electron concentration above the F region, and to a lesser (but nevertheless important) extent by the nearly flat profile of ionization around the bulge of the F region and the curvature of the earth's magnetic field. The high vertical gradient extends to heights above 1000 km for daytime conditions and is a consequence of a scale-height dominated by oxygen and helium ions. For the range of latitudes where erosion is observed, it has been found that the ray trajectories are curves that cross the equator below 1000 km. Hence, the effects of equatorial erosion are observable only by satellites operating below ~1000 km at low latitudes.

Details of the analysis. The equatorial erosion phenomenon can be predicted by a study of D-region absorption, followed by a study of ray trajectories to determine the region of space where the effect should be observed at the satellite.

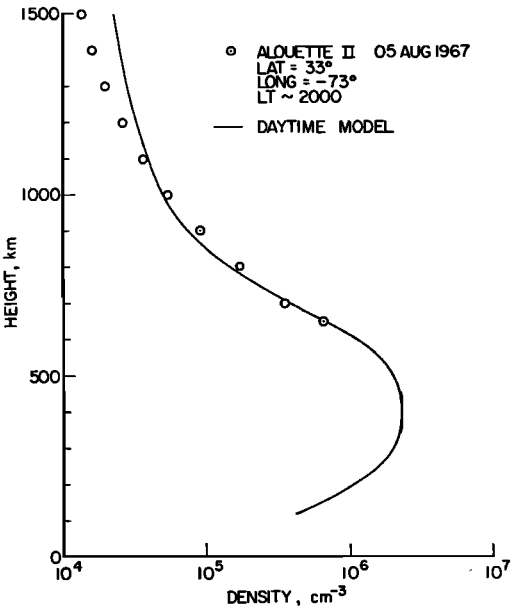

Fig. 3. Daytime equatorial model of the ionosphere above 100 km. Electron-concentration measurements made by Alouette 2 are also shown (data supplied by L. Colin).

The ionospheric model used included the electron collision frequency and density profiles for the daytime D region of *Piggott et al.* [1965]. For heights above 100 km an analytical electron-concentration profile was developed satisfying measurements made by Alouette 2 in August 1967 (data kindly supplied by L. Colin). This profile of ionization is shown in Figure 3 together with Alouette measurements.

The wave equations governing reflection and transmission in the lower ionosphere were numerically integrated by means of a 'full-wave' computer program [*Scarabucci*, 1969]. The main interest here was to determine the transmission coefficient in the lower ionosphere as a function of the magnetic latitude. At each magnetic latitude the direction of the incident wave was chosen so as to give maximum transmission. The polarization at each latitude was selected to be the polarization of the 'penetrating mode,' that is, the incident wave is polarized so as to give the maximum power flow just above the E region of the ionosphere [*Pitteway*, 1965].

The ionosphere was assumed to be planarly stratified up to 150 km. The square of the transmission coefficient T_p is the ratio of the vertical power flow high in the ionosphere and the vertical power flow of the incident penetrating mode. Hence, the total loss (reflection plus absorption) in the lower ionosphere is given by

$$L = 20 \log_{10} T_p \quad \text{db} \qquad (1)$$

This represents the minimum loss, since L is calculated for the angle of incidence that gives maximum T_p. The computer calculation was programmed to stop at 120 km, where the collision frequency is small and where the WKB method can replace the 'full-wave' method. The remaining E-F region absorption is small compared with the D-region absorption and has been neglected. Figure 4 gives the ionospheric loss L as a function of input magnetic latitude for a range of frequencies. The higher frequencies exhibit relatively greater losses, and both the amount of loss and its frequency dependence increase rapidly toward lower latitudes.

Figure 4 shows that if the receiver threshold is constant with frequency, the highest frequen-

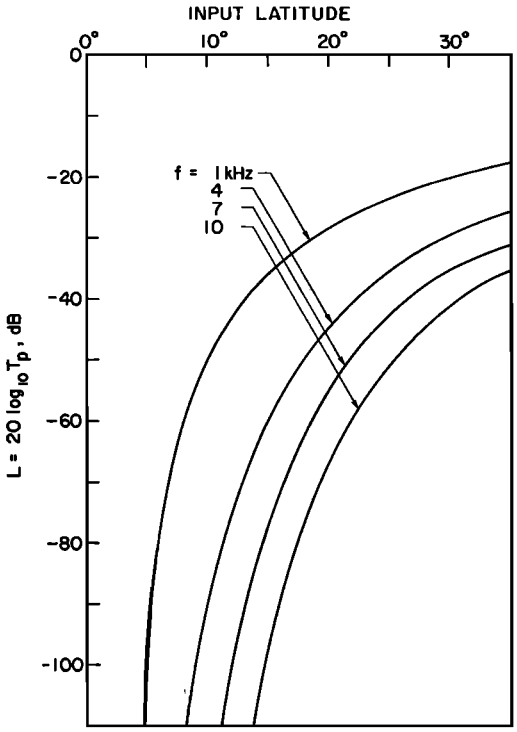

Fig. 4. Total ionospheric loss (reflection plus absorption) as a function of magnetic latitude for several frequencies.

cies should disappear first and the lowest frequencies later for a satellite approaching the equator. Thus the absorption analysis qualitatively explains the equatorial erosion effect.

For daytime ionospheric models the transmission loss is caused almost exclusively by absorption, the amount of loss introduced by reflection being comparatively small. Hence, the behavior shown in Figure 4 could be predicted with a simpler technique. As an example, curves of absorption given by *Helliwell* [1965, Chapter 3], which are based on the integral of the imaginary part of the refractive index, agree reasonably well with Figure 4.

Daytime ray-trajectories around the equator. The next necessary step is to follow the ray trajectories to determine further effects and the satellite positions where the absorption introduced by the lower ionosphere will be detected. Figure 5 shows some 1-kHz ray-paths produced by a ray-tracing computer program [*Walter*, 1969] using the ionospheric model shown in Figure 3. The illustrated rays start at the height of 120 km and at 8°, 10°, 12°, and 14° of latitude with vertical wave normals, as indicated by small arrows. The ray that starts at 8° follows a trajectory well inclined toward the equator because of the guiding effect of the magnetic field that has low dip angles at these latitudes. The result is that a substantial length of the ray trajectory occurs at the height of the bulge region of the *F* region where the vertical gradient of electron concentration is small. Therefore, the rate of change of the wave-normal direction that is primarily dependent on the vertical ionization gradient is also small. Hence the ray proceeds upward until higher gradients of electron concentration are met above 500 km, which then bend the wave-normal downward and the ray returns to the lower ionosphere.

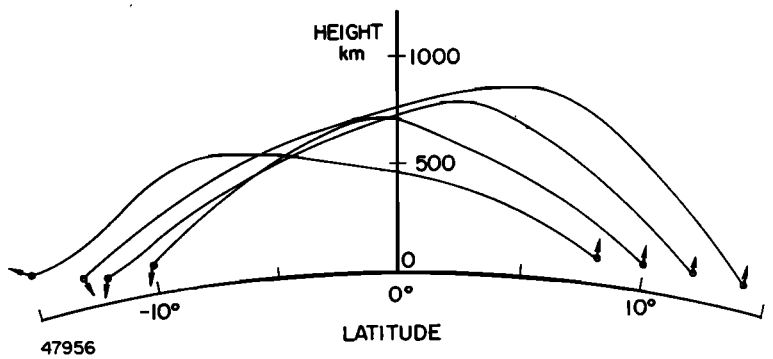

Fig. 5. Ray trajectories for 1-kHz waves in the equatorial ionosphere using the electron-concentration model of Figure 3. The assumed dipole geomagnetic field has an equatorial gyrofrequency of 870 kHz at the ground.

Rays that start above 8° of latitude are affected by magnetic field lines with higher dip angles, and therefore the rays cross the F region less obliquely (see Figure 5). Such rays will be affected by the high electron-concentration gradient above the F region closer to the input latitude for successively higher input latitudes. As a consequence, the apogees of the trajectories move from negative to positive latitudes when the input latitude varies from 8° to 14° as shown in Figure 5. The resulting downgoing rays present the possibility of wave interference because of ray crossings and also some focusing caused by ray bunching. The ray trajectories for wave frequencies between 1 and 10 kHz are almost equal to the curves shown in Figure 5, the maximum difference being approximately half-degree in latitude for some rays at 10 kHz. Therefore, it is only necessary to show the propagation properties displayed by one wave frequency.

Figure 6 shows the relationship between the input latitude at 120 km where 1-kHz rays start and the latitudes where a 600-km polar-orbit satellite would receive the rays (continuous curve) together with the related travel times (dashed curve). Figure 6 is to be used in the following way: Given an upgoing ray at a specified latitude (left side of figure) it will cross the height of 600 km at two latitudes, namely as upgoing wave (section CD) or as downgoing wave (section ABC). For a given satellite latitude the travel times are read on the right side of the figure. For example, a 1-kHz ray that starts at 10° of latitude will be received by the satellite at 2° as upgoing wave with a delay time of 0.76 sec and will be also detected at −3.6° as downgoing wave with 1.10-sec time delay.

Figure 6 shows the fact already described by Figure 5 that the trajectories are not symmetrical around the equator: there is bunching of rays at negative latitudes and some divergence of rays at positive satellite latitudes. Numerical calculations indicate that the above divergence loss and focusing gain represent less than ±3 db, a number that is negligible in comparison with the low ionosphere absorption shown in Figure 4. A strong focusing of rays may occur at the point B where the derivative of the curve is infinite; this point will be discussed later.

Figure 6 also shows that wave interference should occur in a certain range of negative latitudes where rays that come from different starting latitudes are observed at one point. Although this statement is certainly true for a sinusoidal wave of long duration, it requires a further discussion for the case of whistler reception where each wave frequency exists only during a short duration. For example, if the satellite location is −5°, it would receive 3 distinct rays (see Figure 6) whose delay times are 1.090, 1.155, and 1.170 seconds, but the last 2 rays would appear as 2 distinct traces only

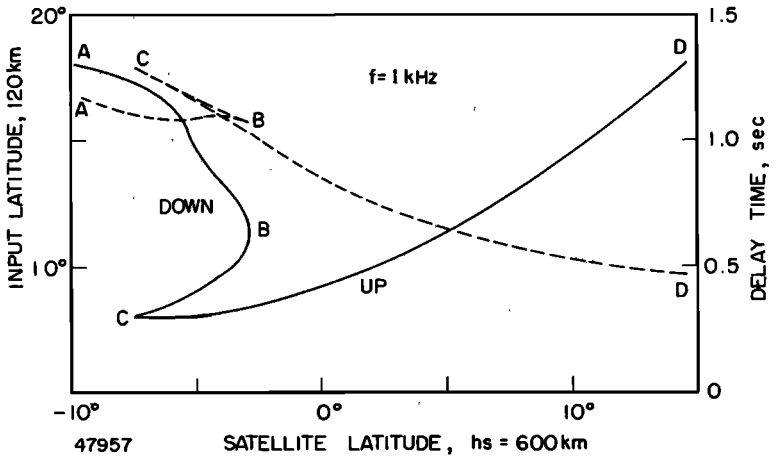

Fig. 6. Input latitudes at 120 km and the related latitudes where 1-kHz rays will be detected by a 600-km polar-orbit satellite. For a given satellite latitude (on the bottom) the related travel time can be read on the right side of the figure (dashed curve).

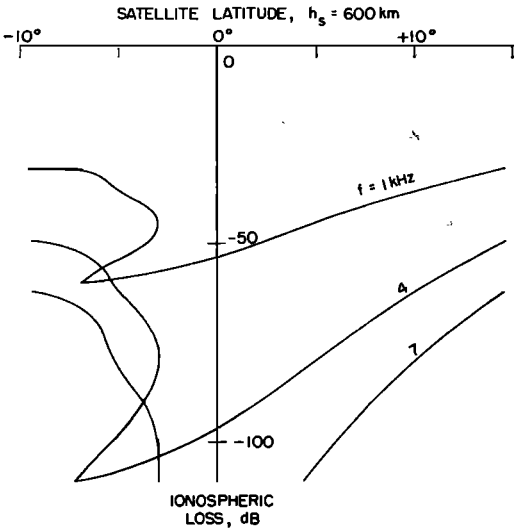

Fig. 7. Ionospheric loss observed by a 600-km polar-orbit satellite as a function of the latitude. The curves are parametric in frequency.

if the duration of the 1-kHz packet is smaller than 15 milliseconds at the receiving point. Otherwise and more generally if two interfering rays are received at the same location, they will produce wave interference only during the period when both packets coexist. The amplitude of the interfering waves may be very different because they were differently affected by the lower ionosphere absorption (as given in Figure 4) although the above effect may be compensated by the position of the lightning source relative to the entry points below the ionosphere. Therefore the complete picture of whistler interference near the equator is somewhat involved depending on several factors, namely ionospheric profile (controlling the delay times and trajectories), frequency, and relative positions of lightning source and satellite. Typical OGO 4 records of downgoing whistlers at low latitudes display fading in the whistler traces as well as the occurrence of almost coincident traces that sometimes merge together. The above features together with the erosion effect are present in the OGO 4 spectrogram of Figure 1 at negative latitudes where downgoing whistlers are being received (see bottom panel).

Using Figure 6 the ionospheric loss of Figure 4 is related to the satellite latitude by going along the ray trajectories up to 600 km. This is shown in Figure 7 for wave frequencies 1, 4, and 7 kHz. Figure 7 shows that the erosion effect should be unsymmetrical around the equator if the lightning sources are located at one side of the magnetic equator. For example, the curve for 1 kHz shows that for a northbound equatorial pass of a 600-km satellite the signal decreases 10 db between −5.4° and −3°. However, this loss is recovered north of the equator between 5° and 11.6°. Figure 7 also shows that the rate of loss with latitude is greater at higher frequencies.

The predicted focusing of the rays at the latitude B of Figure 6 is probably effective only at the low frequencies where ionospheric losses have not been excessively high. The focusing is ineffective at higher frequencies because these waves are absorbed by the lower ionospheric medium.

The asymmetry of the erosion effects around the equator is caused in part by the nonsymmetrical ray trajectories around the equator and partially because of the response of the receiver under different regimes. This is the difference in the response of the satellite receiver to 'short' upgoing whistlers and 'dispersed' downgoing signals and the fact that upgoing whistlers were concentrated north of the magnetic equator and downgoing whistlers on the southern side. In the case of short upgoing whistlers received north of the equator the peak signal is large; the instantaneous AGC of the log-compressor receiver acts to lower the gain so as to reveal some amplitude details (hence the irregular structure of Figure 1) that fall below a certain clip level. In the case of dispersed downgoing whistlers observed south of the equator the signal is on the average relatively weak and of long duration, the AGC action maintains high gain levels with much of the signal near the clip level, and the result is an abrupt change in blackness of the display at the cutoff or beginning of high attenuation.

Equatorial Defocusing

At nighttime the transition height at which the equatorial ionosphere changes from a scale-height dominated by oxygen to a scale-height dominated by hydrogen is usually below 1000 km (see for example, *Prasad* [1968]). Therefore the vertical gradient of electron concentration may change rapidly between the peak of

the F region and 1000 km. In what follows we use the results of a ray-tracing computer program to analyze the effects of this change in ionization gradient upon the propagation characteristics of VLF waves.

Figure 8 shows some ray tracings for typical day- and nighttime electron-concentration profiles. Both daytime and nighttime profiles simulate Alouette 1 topside measurements taken over the equator in November 1962. The ray path shown for the daytime profile (dashed curve) is more or less typical for waves starting between 5° and 15°, i.e., the ray trajectories are approximately symmetric around the equator. In this case the curvature of the earth's magnetic field plus the high vertical gradient of electron concentration above the F region provide a significant rate of change of the wave normal direction all the way along the path. As a consequence the wave normals bend initially toward the equator, cross the equator oriented almost horizontally, and finally bend rapidly inward from the field line direction. These waves arrive in the D region of the conjugate hemisphere with almost vertical wave normals.

The two ray paths shown for the nighttime profile (solid curves) present two types of behavior. The ray path that starts at +9° is typical of waves whose incident latitude is relatively close to the equator. This path is similar to the one presented by the daytime curve, in that the wave normals bend rapidly earthward in the region of high vertical gradient of ionization below 600 km, where the nighttime profile is dominated by the O^+ scale-height. The nighttime ray whose starting latitude is +10° presents a behavior that is typical for rays starting above ~10°, i.e., it crosses the equator above the transition height. As a consequence, the rate of change of the ray direction, which is approximately proportional to the vertical gradient of ionization, is much smaller for this group of rays. Figure 8 shows that in this case the wave normal remains pointing upward over a wide range of latitudes, bends slowly toward the horizontal, and finally bends rapidly earthward when the ray enters the region of low scale-height below the transition height. The differences in the behavior of the ray trajectories presented for the nighttime profile, depending on whether the ray crosses the equator above or below the transition height, produce the defocusing of the rays labeled a and b.

The defocusing phenomenon can be quantitatively analyzed if a relationship is found between the latitudes where the rays start and the latitudes where they should be intercepted by a satellite crossing the equatorial region at constant height. The result of such a calculation is shown in Figure 9 for the nighttime ionospheric model of Figure 8 and for two satellite heights, h_s = 450 and 700 km. Figure 9 shows that rays starting at a given input latitude (the independent variable) may obviously be detected by a satellite in two different ways: as upgoing or as downgoing waves. Arrows indicate the satellite latitudes for which the rays will be detected as upgoing (UP) or downgoing (DOWN) waves. For example, the curve for h_s = 450 km shows that rays whose

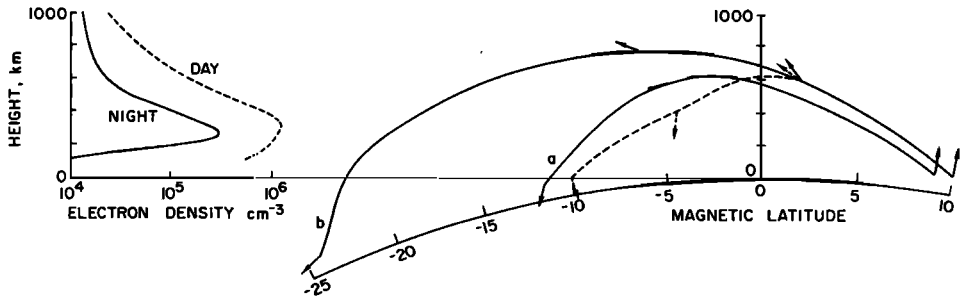

Fig. 8. Typical daytime and nighttime ray trajectories followed by waves of 17.8 kHz near the magnetic equator. The directions of the wave normal are represented by small arrows, showing that the equatorial defocusing occurs when the medium loses the ability of effectively bending down the wave normal. This effect is caused by a weak vertical gradient above the transition height in the nighttime electron-concentration distribution.

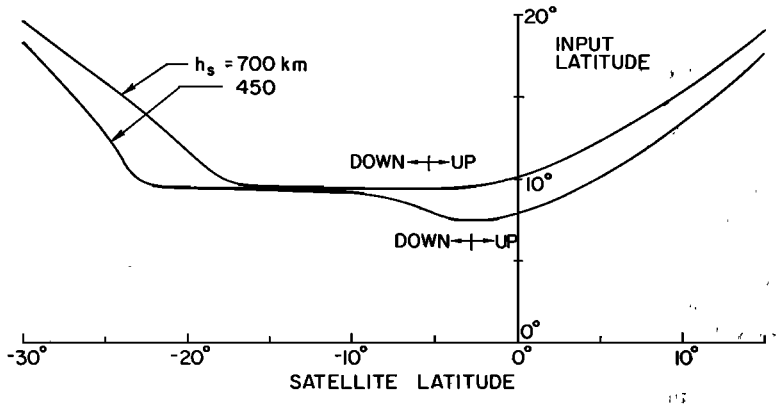

Fig. 9. Correspondence between the latitudes where the rays leak from the earth's waveguide and the latitude where they will be detected by a satellite whose height is h_s. Arrows indicate the regions where upgoing (UP) and downgoing (DOWN) rays are received. The height at the input latitude is 120 km where the wave normals are assumed vertical. The ionospheric model is the nighttime profile shown in Figure 8. The assumed dipole geomagnetic field has an equatorial gyrofrequency of 870 kHz at the ground.

input latitude is 8.5° will intercept the satellite at 2° of latitude as upgoing waves and at −6.5° of latitude as downgoing waves. Little defocusing loss is predicted for these rays. Defocusing loss is apparent where the curves are flat, meaning that there is a very wide range of latitudes where the satellite will be receiving energy that comes from a very narrow range of input latitude. Observe, for example, that rays starting between 9° to 9.6° are upwardly detected between 3° to 4° by a satellite at 450 km and that the corresponding power flux will be weaker in the southern hemisphere because the downgoing rays will be detected from −9° to −22° of latitude.

The focusing gain is defined by the ratio between the input and the output cross section areas of a 'tube of rays.' The tube of rays may be determined by two adjacent rays separated in latitude by $\Delta\phi$, and by a longitudinal decrement $\Delta\lambda$. If we suppose that the rays remain in the same magnetic meridian—a good assumption for very low frequencies—then the focusing gain is independent of $\Delta\lambda$ and is given by

$$G_F = \left(\frac{R_i}{R_s}\right)^2 \cdot \frac{\Delta\phi_i \cos\phi_i \cos\beta_i}{\Delta\phi_s \cos\phi_s \cos\beta_s} \qquad (2)$$

where i refers to the position of input and s to the position of the satellite. Figure 10 shows the geometrical parameters involved in (2): R is the geocentric radius, ϕ is the magnetic latitude, and β is the angle between the ray and the local vertical.

The factor $(\Delta\phi_i/\Delta\phi_s)$ is readily determined from Figure 9, and β is a side product of the ray-tracing computer program. Hence, the focusing gain can be calculated as a function of the latitude of the satellite. This is shown in Figure 11 for ray inputs in the northern hemi-

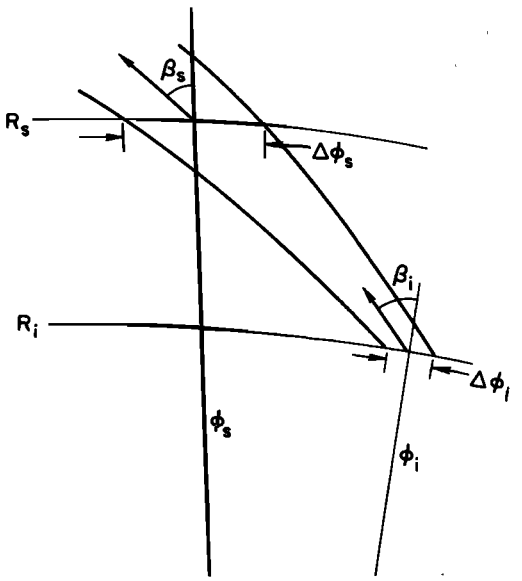

Fig. 10. Tube of rays and geometrical parameters for determining the focusing gain.

sphere and for two different satellite heights, h_s = 450 and 700 km (solid curves). The calculations predict that the drop of the signal will occur when the satellite is in the hemisphere conjugate to that of the transmitter, and that the signal will decrease abruptly in space, in very good agreement with the measurements as shown by the dashed curves. The calculations also indicate that the signal should recover at a slower rate which, again, is usually observed.

To compare the calculated focusing gain with the observations it is necessary to normalize the amplitudes of the measurements made just before the equatorial defocusing. This has been done in Figure 11 by fixing the initial signal level at +2 db and placing the leading edge of the measured defocusing region at −24°. The two consecutive measurements, separated by 25° in longitude, present qualitative similarity but substantial differences in level. For example, Figure 2 shows that at the south of the defocusing region the upper record (longitude −54°) presents smaller field levels compared with the bottom record (longitude −78°). Because of this fact the noise level displayed by the records of Figure 2 inside the defocusing regions is represented in Figure 11 by flat lines 9 db apart, the higher line corresponding to the equatorial pass at the longitude of −54°. Figure 11 shows that the curve predicted for a satellite height of 450 km is the one that reasonably matches the observed defocusing for the pass of LONG = −78°, although OGO 4 height was 730 km. It will be shown that this fact suggests a higher transition height for the ionosphere at −78° of longitude. This point will be discussed in the next section.

Nighttime ionospheric loss. Next, it is proposed to determine the role played by the lower ionosphere during the night. To estimate the leakage of the earth-ionosphere waveguide at different magnetic latitudes the following procedure is taken. The leakage of the dominant waveguide mode $n = 1$ is produced by waves whose angle of incidence in the lower ionosphere is ~80° [*Wait*, 1962]. The full wave computer program is then used in order to determine the transmission loss as a function of the latitude for a constant 80° angle of incidence. The nighttime electron concentration and collision-frequency profiles were taken from *Deeks* [1966]. The result is shown in Figure 12 where the transmission loss is plotted for different input

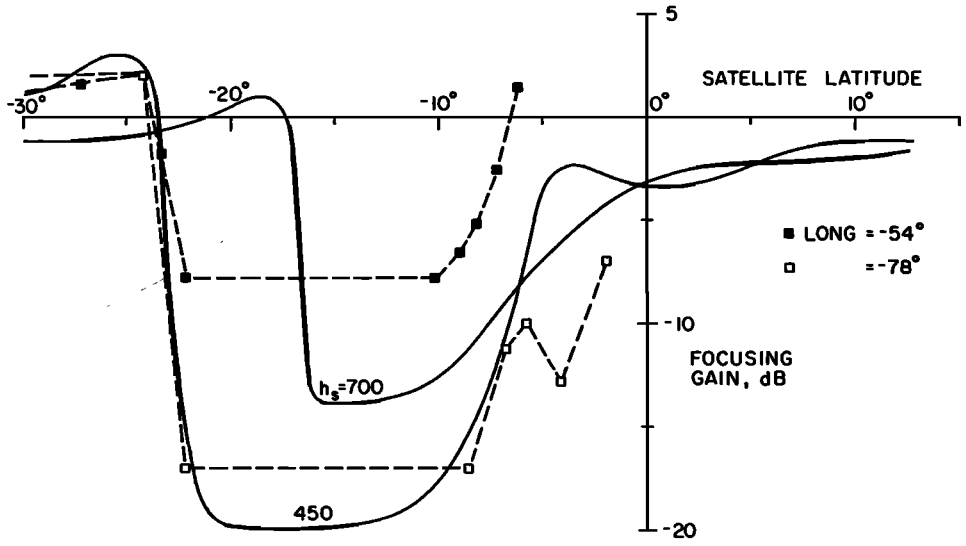

Fig. 11. The continuous curves show the focusing gain as a function of the satellite latitude calculated for two different satellite heights, h_s = 450 and 700 km. The dashed curves represent the measurements shown in Figure 2 (OGO 4 height was 730 km at both equatorial crossings). For these experimental curves the relative starting signal level has been normalized to +2 db and the leading edge of the defocusing region has been placed at −24°.

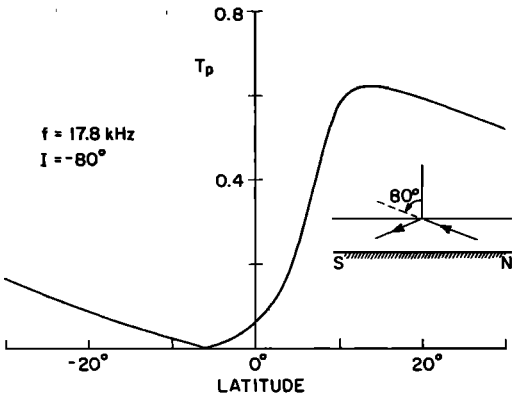

Fig. 12. Lower-ionosphere transmission coefficient for penetrating mode waves traveling southward. The propagation is supposed to be in the magnetic meridian, and the angle of incidence is −80° as indicated in the sketch by the curve.

latitudes and for southward traveling waves from NAA. It shows that the transmission coefficient is maximum at ~14° latitude, experiences a sharp decay at latitudes below 10°, and falls to zero at −6° latitude. In the southern hemisphere the transmission coefficient recovers slowly, reaching significant values again only for latitudes below −45°. These abnormally low values for the transmission coefficient come from the fact that at ionospheric heights where the wave normals are changing direction from −80° to almost vertical, the wave normal crosses a region of high collision frequency while making an angle of nearly 90° with the earth's magnetic field. Figure 12 is in good qualitative agreement with a similar study made by *Pitteway and Jespersen* [1966] for a different low ionosphere. Figure 12 leads to three conclusions:

1. The sharp decay of the transmission coefficient below 10° does not interfere with the equatorial defocusing, because the satellite height is such that it will only receive rays starting above ~9° of latitude (see Figure 9).
2. Between 0° and −20° latitude the transmission coefficient is so small that signals coming from below cannot be detected in the defocusing region of Figure 11.
3. The region of high transmission coefficient for whistlers excited from one side of the equator coincides with the low transmission coefficient region for whistlers excited on the opposite hemisphere and vice versa.

Conclusions 1 and 2 substantiate the results previously provided by the ray-tracing technique, i.e. we should observe a region of defocusing for waves starting below the ionosphere and coming from one side of the equator.

Conclusion 3 states that the equatorial erosion cannot be observed during the night because the defocusing region for whistlers generated in one hemisphere is filled with upgoing whistlers from the other hemisphere and vice versa. We should only observe a short dispersion characteristic for whistlers inside the defocusing region corresponding to upgoing whistlers. This phenomenon has been observed.

Factors Affecting the Equatorial Defocusing

As we pointed out previously the equatorial defocusing is directly related to the change of the electron-concentration scale-height at the transition height. Between the peak of the F region and the $[O^+ - H^+]$ transition height the vertical density gradient is usually high because

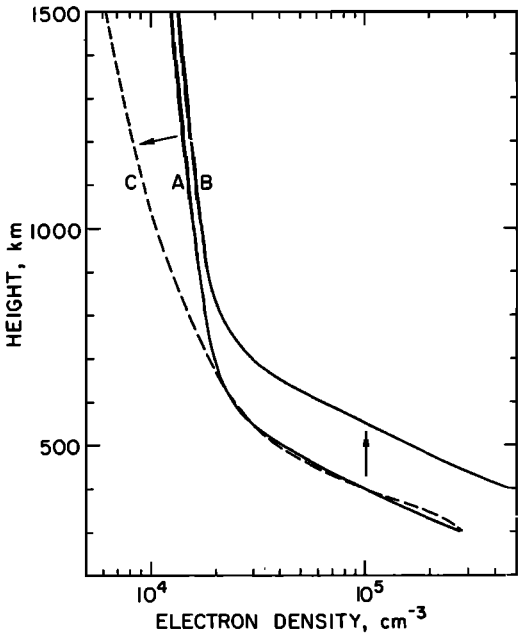

Fig. 13. Three ionospheric models A, B, and C. Model A is the nighttime model of Figure 8. Model B is obtained from A by increasing the transition height. Model C has a hydrogen scale-height 70% of the hydrogen scale-height of model A.

the electron scale-height is almost exclusively given by the scale-height of O^+. As a consequence the ray trajectories below the transition height remain reasonably unchanged for different ionizations. For example, the nighttime and the daytime ray trajectories shown in Figure 8 are exactly the same below the nighttime transition height although the two ionospheric profiles present substantially different electron-concentration levels.

Above the transition height the defocusing is controlled by the H^+ scale-height. A smaller H^+ scale-height produces a smaller defocusing loss. Another very important factor is the smoothness of the transition from the O^+-dominated region to the H^+-dominated region. If enough helium is present, the transition region is smoothed out because the He^+ scale-height is only 4 times greater than the O^+ scale-height. A smooth transition profile around the transition height produces a smaller defocusing loss. Hence, a strong equatorial defocusing is an indication that the He^+ concentration around the transition height is necessarily very small.

To give a numerical treatment to the above discussion we shall consider the three different ionospheric models A, B, and C shown in Figure 13. The ionospheric models have been calculated assuming a diffusive equilibrium distribution [*Angerami and Thomas*, 1964]. Profile A is the nighttime model previously shown in Figure 8. This model has an H^+ scale-height of 1600 km (i.e., a neutral H scale-height of 800 km). Profile C has an H^+ scale-height of 1120 km, namely 70% of the H^+ scale height presented by profile A. Profile B is obtained from A, essentially increasing the transition height by about 150 km. Figure 14 is the result of several ray-tracing computations showing the satellite latitude where the rays will be detected as a function of the latitudes where they start. Curves for the ionospheric models B and C are shown where the satellite height has been assumed equal to 700 km. These results can be compared with the results for profile A shown in Figure 9. Figure 14 indicates that the ionospheric model C gives no substantial defocusing (observe the derivative $d\phi_s/d\phi_i$). Calculations show that the maximum defocusing for this model is around 5 db for a satellite height of 700 km. In contrast, profile B produces a strong defocusing as we should expect because the corresponding electron concentration distribution is essentially the same as profile A but vertically shifted. Observe that the B curve in Figure 14 resembles the curve corresponding to $h_s = 450$ km in Figure 9. Figure 15 gives the focusing gain for this ionospheric model B as a function of the satellite latitude for $h_s = 700$ km. Notice that the calculated defocusing region has a length very similar o he one presened by the curve for $h_s = 450$ km in Figure 11. This indicates that we can effectively modify the ionospheric model in order to obtain a prescribed result. Another feature introduced by profile B relative to profile A is a northward shifting of $\sim 5°$ in the position of the defocusing region and a fraction of db in loss (compare with Figure

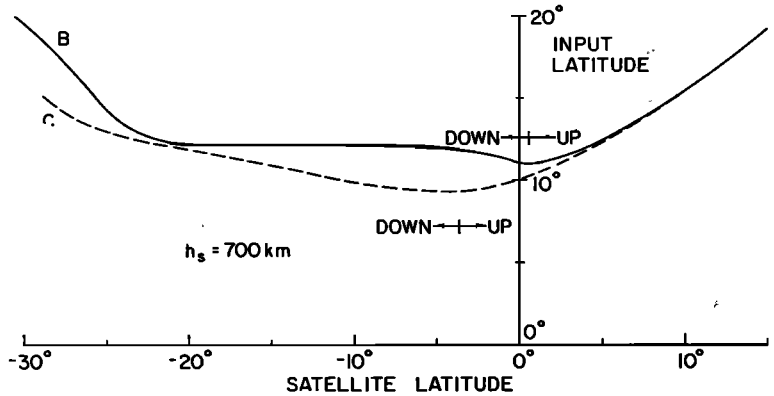

Fig. 14. Correspondence between the latitudes where the rays leak from the earth's waveguide and the latitude where they will be detected by a satellite at 700 km for the two ionospheric models B and C. Compare with the curves derived for model A in Figure 9.

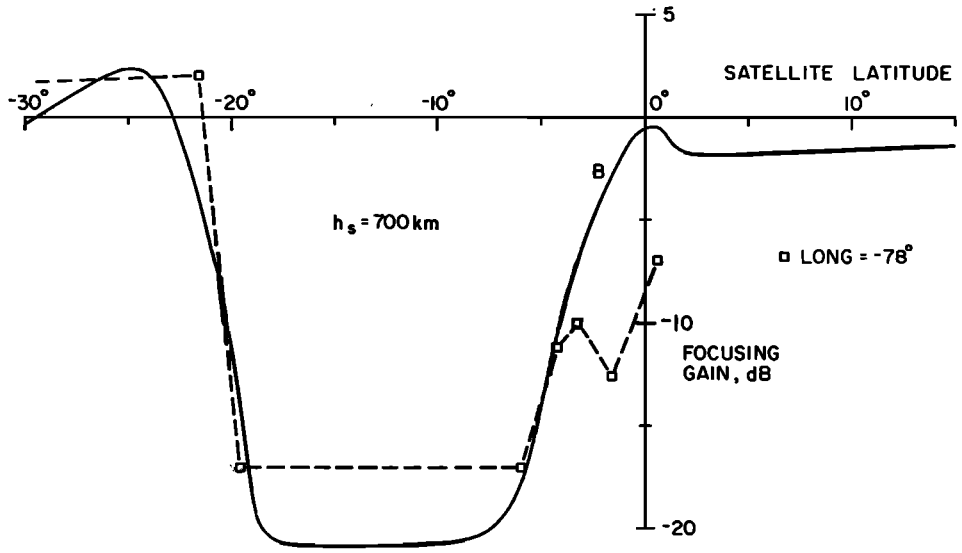

Fig. 15. The continuous curves show the focusing gain as a function of the satellite latitude for ionospheric model *B*. The dashed curve represents one of the measurements shown in Figure 2. For the experimental curve the starting signal level has been normalized to +2 db, and the leading edge of the defocusing region has been placed at −24°.

11). In Figure 15 we also show the satellite measurements for the equatorial pass corresponding to LONG = −78°. Now a very good agreement is obtained.

The transition height for model *B* is 750 km, a value that suits the extrapolation of the midnight transition height curves given by *Prasad* [1968] which were based on the analysis of frequency spectrum of radar backscatter signals from the ionosphere.

A discrepancy still remains, namely that the place of the calculated defocusing region in about 10° southward shifted relative to the measured defocusing region of Figure 2. This point will be discussed in the next section.

Seasonal Variation of the Equatorial Defocusing

Measurements of the equatorial defocusing between November 1967 and July 1968 suggest a seasonal variation in the magnetic latitudes where the equatorial defocusing takes place. This is shown in Figure 16 where the defocusing region is indicated by the position of vertical bars along some satellite passes. They show that the defocusing region for transmitters located in the northern hemisphere occurs just below the magnetic equator (as predicted) for months in which the sun's declination is negative. For months of positive sun's declination (northern hemisphere summer) the defocusing region seems to move northward. A detailed study of this northward shift is difficult because the passes shown in Figure 16 have occurred at different local times as illustrated in the same figure by the numbers below each date. Therefore, it is speculative whether the northward shift presented in Figure 16 is caused only by a seasonal variation in the ionosphere or whether they are more influenced by the local time. Nevertheless, based only on the propagation properties of the waves, it is suggested that the northward shift of the defocusing region during the northern hemisphere solstice is caused by horizontal gradients of electron concentration near the magnetic equator. The direction of the latitudinal gradient for obtaining this effect should be northward, in accordance with electron concentration measurements made by *Reddy et al.* [1967]. This problem can be analyzed when a more complete seasonal behavior of the equatorial defocusing is known.

Conclusions

In this paper we have presented the equatorial erosion and the equatorial defocusing of

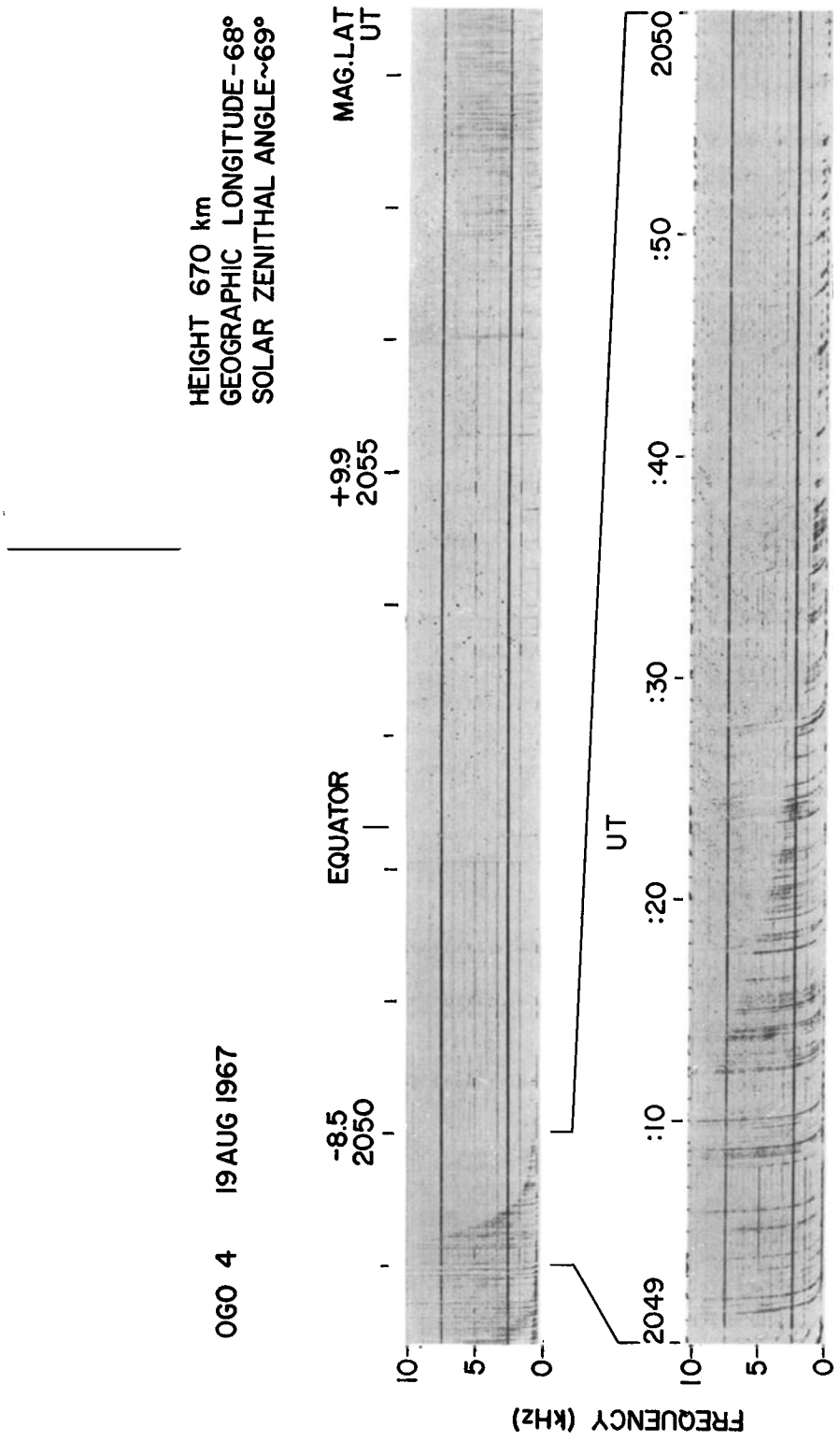

Fig. 1. Frequency-time spectra of broadband VLF data from OGO 4 showing a typical example of daytime 'equatorial erosion.' The bottom panel shows a portion of the upper record in expanded time scale where downgoing whistlers that enter the ionosphere in the conjugate hemisphere exhibit a latitude-dependent upper cutoff. The horizontal lines are caused by interference from the odd harmonics of the spacecraft dc converters at 2461 kHz (heavy lines) and harmonics from the 800-Hz power supply line (weak lines) that show up when the external signal level is very low.

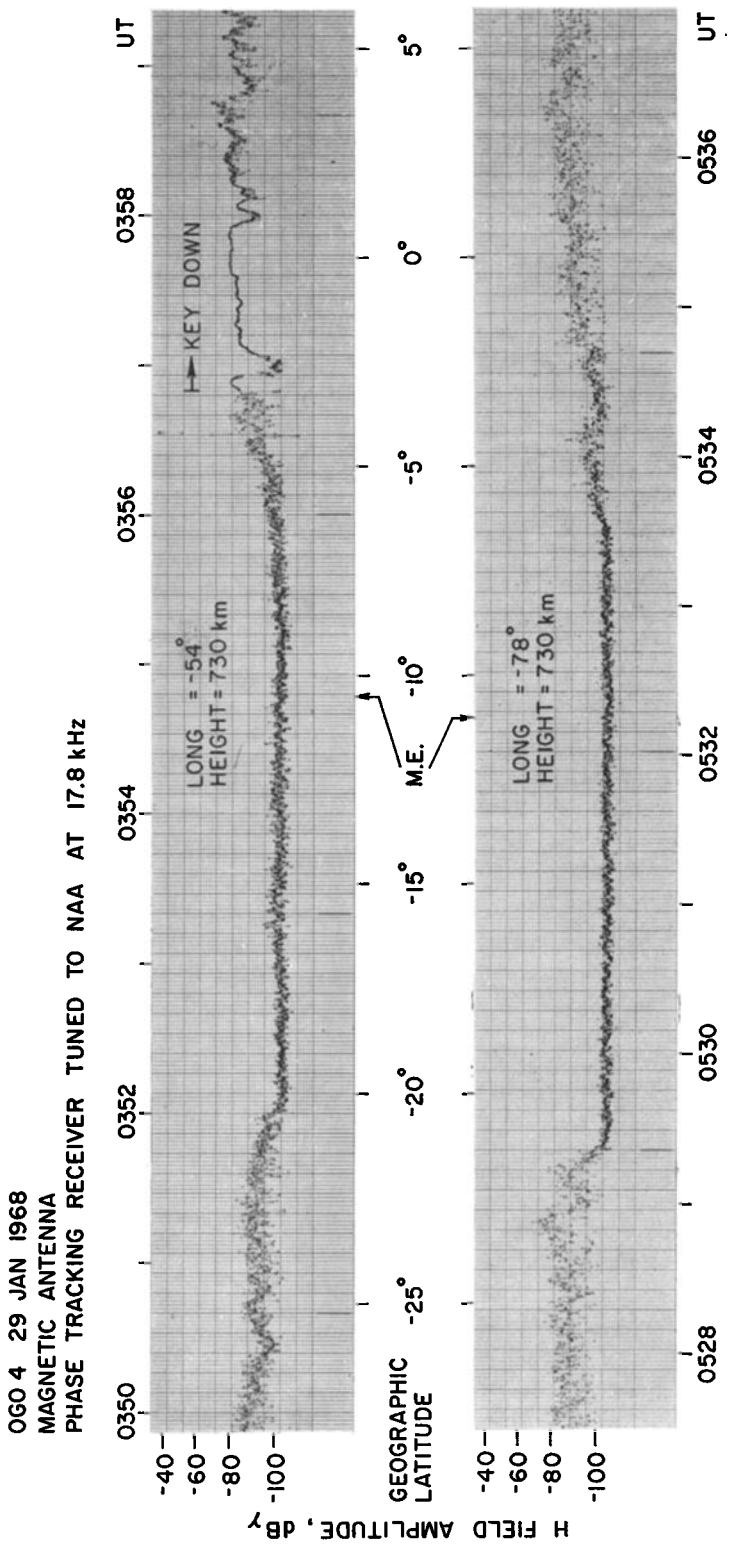

Fig. 2. OGO 4 records showing the NAA magnetic field amplitude as measured by the satellite phase-tracking receiver in two consecutive equatorial crossings. The records present the nighttime 'equatorial defocusing' with the amplitude of the signal dropping below equipment threshold at about −100 dbγ. The relative position of the magnetic equator is indicated by M.E. At about 0357 UT the pattern of NAA signal changes to Key-Down mode, preceding the major change from CW (0300–0400 UT) to FSK (0400–0500 UT) in the mode of transmission.

VLF waves propagating at low magnetic latitudes. It has been shown that the equatorial erosion is caused by ionospheric losses (absorption plus reflection) in the D region. These losses increase for lower latitudes and may cause the complete disappearance of all VLF waves from the receiver of a low altitude satellite. During the night, absorption is less important, but nevertheless a very pronounced drop in the signals of VLF transmitters has been observed. We showed that this new phenomenon is caused by ionospheric defocusing of VLF rays near the magnetic equator. This defocusing is related to the change of the vertical gradients of the electron concentration distribution that takes place around the transition height. A full-wave treatment has been applied to the propagation through the lower nighttime ionosphere. This study confirmed the defocusing interpretation by showing that upgoing rays were prevented from reaching the defocusing region by excessive ionospheric loss in the lower ionosphere. Finally we showed that the ionospheric model can be modified to obtain a prescribed equatorial defocusing pattern. Given the satellite height we can approximately state: (1) The amount of the defocusing loss can only be achieved with a hydrogen scale-height greater than a specified value; (2) the width of the defocusing region determines the minimum height of the transition region of the ionosphere; (3) the position of the defocusing region relative to the magnetic equator will be a measure of the horizontal gradient in the ionosphere. Although these three steps are not completely independent, they change the equatorial defocusing in the way indicated above.

The above process of matching a measured defocusing loss by suitable changes in a basic ionospheric distribution represents a potential diagnostic tool for obtaining the $[O^+ - H^+]$ transition height and the hydrogen temperature in the equatorial ionosphere. As pointed out previously the defocusing phenomenon is highly sensitive to the height of the $[O^+ - H^+]$ transition and hydrogen temperature just above that height. On the other hand, the phenomenon is relatively unaffected by different electron distributions below the transition height (compare, for example, the upgoing sections of the ray trajectories for nighttime and daytime profiles of Figure 8). Therefore, in order to fit a speci-

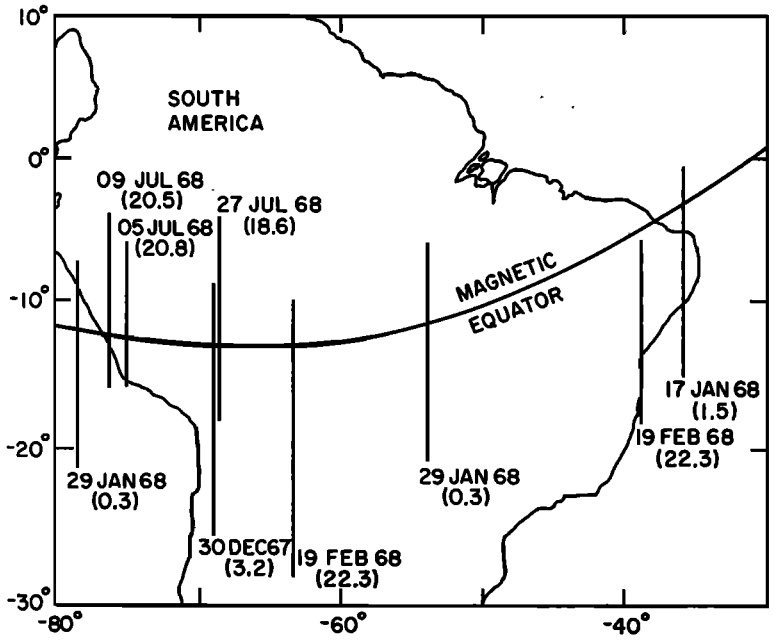

Fig. 16. Position of the defocusing region relative to the magnetic equator. The figure suggests a northward movement of the defocusing region in the northern hemisphere summer months. The number below each date is the local time at the crossing of the equator.

fied defocusing measurement the most important parameters are the transition height and hydrogen temperature, regardless of possible discrepancies between the assumed profile and the actual ionospheric profile. Further development of this propagation method could provide indirect measurements whose accuracies might compete with presently available processes of measuring transition height and temperature. Obviously the suggested method can only be applied at the magnetic equator and during nighttime because there is no significant defocusing during the day. However, the process would provide measurements at all longitudes, and the cost of analyzing the data is relatively low.

Acknowledgment. The author is greatly indebted to Professor R. A. Helliwell and his colleagues for helpful discussion and criticism of the manuscript.

This research was supported in part by the National Aeronautics and Space Administration under contract NAS 5-3093 and grant NGL-05-020-008, and in part by the National Science Foundation Office of Computer Sciences under grant NSF GP-948. The work was carried out under a graduate student research assistantship awarded by Stanford University and a scholarship awarded by C.N.A.E.-Brazil.

References

Angerami, J. J., and J. O. Thomas, Studies of planetary atmospheres, 1, The distribution of electrons and ions in the earth's exosphere, *J. Geophys. Res., 69,* 4537, 1964.

Deeks, D. G., *D*-region electron distributions in middle latitudes deduced from the reflexion of long radio waves, *Proc. Roy. Soc. A, 291,* 413, 1966.

Helliwell, R. A., *Whistlers and Related Ionospheric Phenomena,* Stanford University Press, Stanford, California, 1965.

Heyborne, R. L., Observations of whistler-mode signals in the OGO satellites from VLF ground station transmitters, *Tech. Rept. SEL-66-094, Radioscience Lab., Stanford Electronics Labs., Stanford University, Stanford, Calif.,* November 1966.

Leiphart, J. P., R. W. Zeek, L. S. Bearce, and E. Toth, Penetration of the ionosphere by very-low-frequency radio signals-interim results of the Lofti experiment, *Proc. IRE, 50,* 6, 1962.

Piggott, W. R., M. L. V. Pitteway, and E. V. Thrane, The numerical calculation of wave fields, reflexion coefficients, and polarizations for long radio waves in the lower ionosphere, 2, *Phil. Trans. Roy. Soc., London, A, 257,* 243, 1965.

Pitteway, M. L. V., The numerical calculation of wave fields, reflexion coefficients and polarizations for long radio waves in the lower ionosphere, 1, *Phil. Trans. Roy. Soc., London, A, 257,* 219, 1965.

Pitteway, M. L. V., and J. L. Jespersen, A numerical study of the excitation, internal reflection and limiting polarization of whistler waves in the lower ionosphere, *J. Atmospheric Terrest. Phys., 28,* 17, 1966.

Prasad, S. S., Nighttime ionic composition and temperature over Arecibo, *J. Geophys. Res., 73,* 6795, 1968.

Reddy, B. M., L. H. Brace, and J. A. Findlay, The ionosphere at 640 kilometers on quiet and disturbed days, *J. Geophys. Res., 72,* 2709, 1967.

Rorden, L. H., R. A. Helliwell, and R. L. Smith, An interpretation of LOFTI-I VLF observations, *AGARDOGRAPH 74,* Pergamon Press, New York, 1964.

Scarabucci, R. R., Analytical and numerical treatment of wave-propagation in the lower ionosphere, *Tech. Rept. SEL-69-046, Radioscience Lab., Stanford Electronics Labs., Stanford University, Stanford, Calif.,* August 1969.

Wait, J. R., *Electromagnetic Waves in Stratified Media,* Pergamon Press, New York, 1962.

Walter, F., Nonducted VLF propagation in the magnetosphere, *Tech. Rept. SEL-69-061, Radioscience Lab., Stanford Electronics Labs., Stanford University, Stanford, Calif.,* October 1969.

(Received July 24, 1969.)